ESC European Society of Cardiology

Cardiovascular Research (2020) **116**, 1700–1709
doi:10.1093/cvr/cvz310

Delineating the molecular and histological events that govern right ventricular recovery using a novel mouse model of pulmonary artery de-banding

Mario Boehm[1,2,3], Xuefei Tian[1,2], Yuqiang Mao [1,2,4], Kenzo Ichimura [1,2], Melanie J. Dufva[5,6], Khadem Ali [1,2], Svenja Dannewitz Prosseda[1,2], Yiwei Shi[1,2], Kazuya Kuramoto[1,2], Sushma Reddy [7,8], Vitaly O. Kheyfets[5,6], Ross J. Metzger[2,7], and Edda Spiekerkoetter [1,2,8]*

[1]Division of Pulmonary and Critical Care Medicine, Department of Medicine, Stanford University, 300 Pasteur Drive, Grand Bld Rm S126B, Stanford, CA 94305, USA; [2]Vera Moulton Wall Center for Pulmonary Vascular Disease, Stanford School of Medicine, Stanford University, Stanford, CA, USA; [3]Department of Internal Medicine, Universities of Giessen and Marburg Lung Center (UGMLC), Justus-Liebig University Giessen, German Center for Lung Research (DZL), Giessen, Germany; [4]Department of Thoracic Surgery, Shengjing Hospital, China Medical University, Shenyang, China; [5]Department of Bioengineering, University of Colorado Denver, Denver, CO, USA; [6]Section of Cardiology, Department of Pediatrics, Children's Hospital Colorado, Denver, CO, USA; [7]Division of Cardiology, Department of Pediatrics, Stanford University, Stanford, CA, USA; and [8]Cardiovascular Institute, Stanford University, Stanford, CA, USA

Received 27 March 2019; revised 8 October 2019; editorial decision 10 November 2019; accepted 14 November 2019; online publish-ahead-of-print 18 November 2019

Time for primary review: 20 days

Aims The temporal sequence of events underlying functional right ventricular (RV) recovery after improvement of pulmonary hypertension-associated pressure overload is unknown. We sought to establish a novel mouse model of gradual RV recovery from pressure overload and use it to delineate RV reverse-remodelling events.

Methods and results Surgical pulmonary artery banding (PAB) around a 26-G needle induced RV dysfunction with increased RV pressures, reduced exercise capacity and caused liver congestion, hypertrophic, fibrotic, and vascular myocardial remodelling within 5 weeks of chronic RV pressure overload in mice. Gradual reduction of the afterload burden through PA band absorption (de-PAB)—after RV dysfunction and structural remodelling were established—initiated recovery of RV function (cardiac output and exercise capacity) along with rapid normalization in RV hypertrophy (RV/left ventricular + S and cardiomyocyte area) and RV pressures (right ventricular systolic pressure). RV fibrotic (collagen, elastic fibres, and vimentin^{+} fibroblasts) and vascular (capillary density) remodelling were equally reversible; however, reversal occurred at a later timepoint after de-PAB, when RV function was already completely restored. Microarray gene expression (ClariomS, Thermo Fisher Scientific, Waltham, MA, USA) along with gene ontology analyses in RV tissues revealed growth factors, immune modulators, and apoptosis mediators as major cellular components underlying functional RV recovery.

Conclusion We established a novel gradual de-PAB mouse model and used it to demonstrate that established pulmonary hypertension-associated RV dysfunction is fully reversible. Mechanistically, we link functional RV improvement to hypertrophic normalization that precedes fibrotic and vascular reverse-remodelling events.

* Corresponding author. Tel: +1 650 724 1493; fax: +1 650 725 1008, E-mail: eddas@stanford.edu

Graphical Abstract

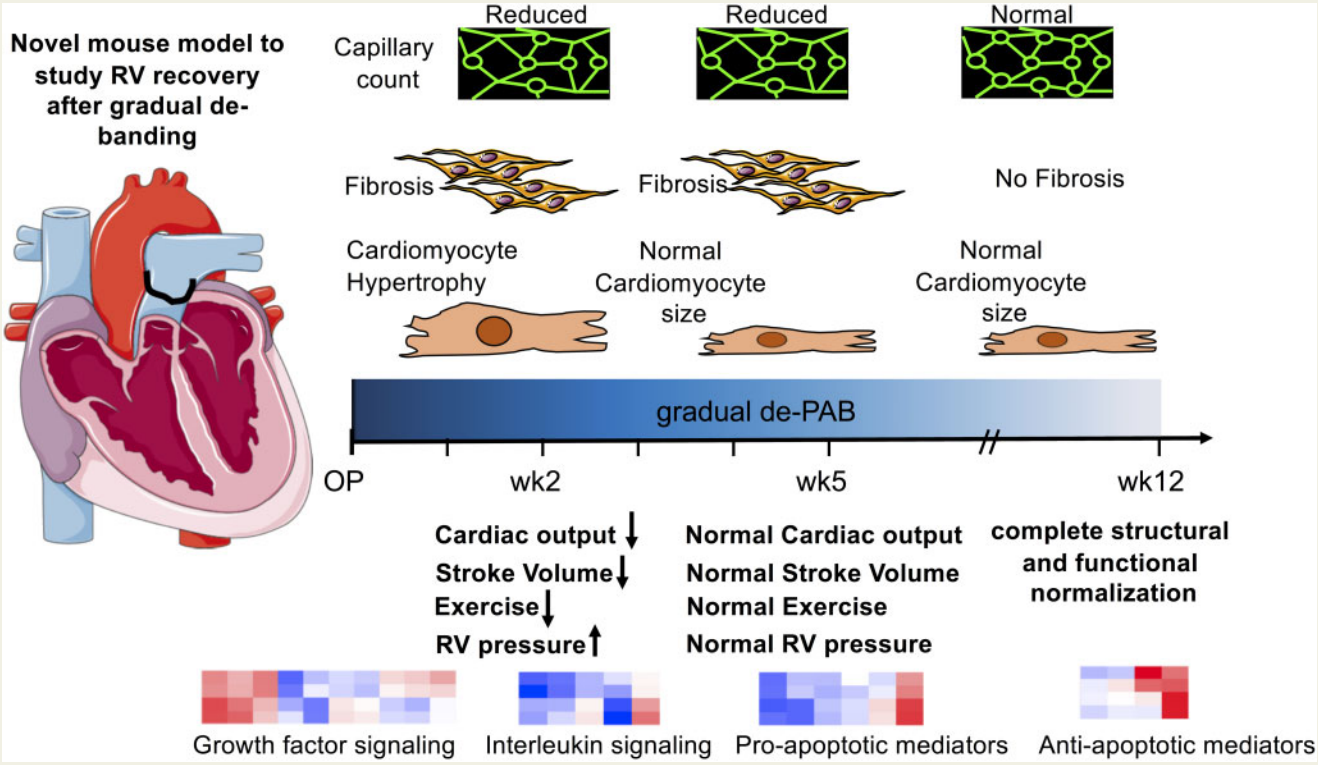

Keywords Pulmonary hypertension • Right ventricle • Recovery • Fibrosis

1. Introduction

Pulmonary arterial hypertension (PAH) is a severe life-threatening disease characterized by a progressive increase in pulmonary vascular resistance that sustainably elevates right ventricular (RV) afterload.[1] The ability of the RV to compensate for changes in load is the single most important prognostic determinant of survival in patients suffering from PAH[2]; and RV failure due to pressure overload is the predominant cause of death.[3] PAH ultimately leads to RV failure in most patients[2]; a subgroup of patients, however, compensates for the increase in afterload over the long-term through RV hypertrophy, with preserved RV function and without RV failure.[4] Why these patients are capable of adapting to high increases in afterload is unknown but it suggests that there are intrinsic RV properties that govern RV adaptation and potentially also RV recovery. Whether the RV should be a therapeutic target in PAH is a controversial topic as the ideal approach to prevent RV failure would be to decrease the elevated afterload.[5] The RV possesses a remarkable ability to recover once the afterload burden is relieved[6,7] even when its function is severely compromised, such as in end-stage PAH when patients undergo lung transplantation.[8–10] Yet, some transplant centres prefer a heart–lung instead of lung transplantation in cases when RV function is severely impaired[11] because knowledge is lacking whether a point of 'no-full-recovery' exists and whether fibrotic and vascular myocardial remodelling are completely reversible once the increased afterload burden is relieved.[12,13]

In the present study, we sought to combine the pre-clinical mouse model of surgical pulmonary artery banding (PAB),[14,15] that was established to study changes in the RV myocardium in response to an increased RV afterload and to test therapeutic approaches that target the RV directly without the interfering afterload alteration from effects on the pulmonary vasculature, with a reversal approach we termed 'de-PAB'. We employed absorbable sutures that possess well-defined hydrolysis kinetics in order to develop a novel pre-clinical animal model for studies on gradual RV recovery from pressure overload. To our knowledge, the data herein are the first to demonstrate the feasibility of gradual cardiac unloading via suture absorption in mice, to identify key molecular components underlying functional RV recovery and to delineate the order and timing of RV reverse-remodelling events with the ultimate goal to understand the RV recovery process and identify ways how to support the RV during recovery.

2. Methods

2.1 Study approval

All animal experiments were performed in accordance with National Research Council guidelines (*Guide for Care and Use of Laboratory Animals*) and approved by local authorities (APLAC, Stanford University, Protocol #27626). Experiments were conducted in a blinded fashion whenever possible (i.e. exercise testing, haemodynamics measurements, or histological analysis).

2.2 Study protocol

Male C57BL/6 mice (10–14 weeks of age) underwent either PAB around a 26-G needle to induce RV pressure overload or sham surgery.[16] Only male mice were used to reduce experimental variability after PAB. All

mice pre-emptively received 0.05–0.1 mg/mg Buprenorphine subcutaneously along with continuous Isoflurane (2–3%) anaesthesia during surgery. PAB was performed with either non-absorbable (silk, hereafter referred to as PAB) or absorbable [VICRYL rapide™ and VICRYL coated® (polyglactin 910), both Ethicon, hereafter referred to as 'rapide' and 'coated', respectively] sutures. Rapide sutures retain ~50% of the original tensile strength at 5 days post-implantation and begin to disintegrate at Day 7–10. All of the original tensile strength is lost by ~10 to 14 days. Absorption is essentially complete by 42 days. Coated sutures retain ~75% of the original tensile strength at 14 days post-implantation. Approximately 50% is retained at 3 weeks, 25% at 4 weeks. All of the original tensile strength is lost by 5 weeks post-implantation and absorption are complete by 56–70 days.[17] Only animals with a peak pressure gradient (PPG) across the PA band greater than 15 mmHg (measured by echocardiography, GE Vivid 7) as assessed one week after surgery were included into the study protocol, with weekly echocardiograms (supine position; continuous 1.5–2% Isoflurane inhalation) and exercise testing (ramped protocol on a rodent treadmill, Columbus instruments)[18] over 5 weeks and at 12 weeks after surgery. We started off with successful surgeries for 16 Sham animals, 14 permanently PA banded, 15 rapide, and 15 coated PA banded mice and excluded animals with a PPG <15 mmHg. Due to additional loss of animals during surgery and also during the first 5 weeks (PAB animals only), we added additional animals ($n = 3$–4 mice per group and timepoint). The sonographer was unsuccessful in acquiring PPG measures at 1 week after surgery in two animals with a coated band and therefore data for only 13 mice were shown in the respective plot (*Figure 1A*). However, longitudinal data were acquired of those animals and PPG indices at the 2-, 3-, 4-, and 5-week timepoint were successfully determined (see *Figure 2A*), therefore, these animals were included in the analysis. At Week 2 and 5 after surgery, mice were assigned to terminal intra-cardiac catheterization[19] (good overall condition is demonstrated by catheter-derived heart rate (HR) measurements, Supplementary material online, *Figure S4*) using their individual pulmonary valve velocity time integral (PV VTI), spanning the entire intra-group range without significant differences in mean PV VTI among all groups to assure that the groups of animals sacrificed at each timepoint had an equal number of equally sick animals.

Of note, data for $n = 2$ coated (wk1) and $n = 2$ sham mice (wk2) were excluded from analysis due to poor ultrasound image quality. Terminally, all mice were euthanized under continuous isoflurane anaesthesia (3–5%) by exsanguination and the RVs dissected for tissue weight measurements.

2.3 Ultrasound image analyses

RV stroke volume (SV) and RV cardiac output (CO) were computed using pulsed waveform Doppler echocardiography. RV outflow tract (RVOT) diameter was measured in four-chamber view by measuring the length of inner edge to inner edge of the pulmonary valve annulus at mid-systole. RVOT area was then calculated as $\pi*(\text{diameter}/2)^2$. RV velocity time integral (VTI) was determined by tracing the RVOT velocity waveform for one ejection period for measurement of area under the curve. This measurement was repeated for two beats and averaged for VTI. SV was calculated as the product of RVOT area and VTI (SV = RVOT area*VTI). CO was then calculated as the product of SV and HR (CO = SV*HR).

2.4 Histomorphology

Cardiac tissues, formalin-fixed, dehydrated, paraffin-embedded, and sectioned (3 µm) were stained by either Masson's trichrome stain, Elastic van Giesson's stain (EVG), wheat germ agglutinin (WGA), Isolectin B4 [IB4; Griffonia Simplicifolia Lectin (GSL I)] (both Vector Labs), Vimentin (ab92547, Abcam), alpha-smooth muscle Actin (aSMA; C6198, Sigma Aldrich), or Periostin (HPA012306, Sigma) as described.[20] Fibrosis was quantified in the RV of Masson's trichrome stained sections by ImageJ area fraction analysis. For cardiomyocyte area calculations and capillary density assessment, more than three images from cross-sectional areas of different RV regions, co-stained with WGA and IB4, were acquired and all events (cardiomyocyte number, cardiomyocyte cross-sectional area, and vessel number) quantified using ImageJ. Capillary density was plotted as ratio of IB4-positive vessels to cardiomyocyte number. Cross-sections of the main pulmonary artery were stained with a Movat-Pentachrome protocol (Histo-Tec, Hayward, CA, USA).

2.5 Gene array and mRNA expression measurements

RNA was isolated from snap frozen, homogenized RV tissue using the Qiagen RNeasy mini kit. Bioanalyzer quality control analysis was performed (RIN scores >5) and samples were subjected to a ClariomS gene array reaction (Thermo Fisher Scientific, Waltham, MA, USA). Automated raw data quality control and analysis was performed using the Transcriptome Analysis Console (TAC, Thermo Fisher Scientific, Waltham, MA, USA) along with GOrilla gene ontology pathway analysis. Venn diagram represents differentially regulated genes ($P < 0.05$, fold change < -2 or >2) for each possible comparison. Heat map data are shown as log2 gene expression values when comparing 2 vs. 5 weeks rapide suture.

Total RNA was extracted and purified from RV tissues with the RNAeasy Plus Kit (Qiagen, Hilden, Germany) and then reverse transcribed using SuperScript III (Invitrogen, Carlsbad, CA, USA) per the manufacturer's instructions. Expression levels of selected genes were quantified using pre-verified Assays-on-Demand TaqMan primer/probe sets (Applied Biosystems, Foster City, CA, USA) and normalized to *Gapdh*.

2.6 Statistics

All data are presented as mean ± standard deviation. We performed statistical analyses using either unpaired two-tailed Student's *t*-test for comparison of two groups or (repeated) one-way or two-way analysis of variance (ANOVA) for comparison of more than two groups followed by Tukey's *post hoc* test if appropriate. Statistical significance was considered to be $P < 0.05$.

3. Results

3.1 PAB impairs RV function and exercise capacity along with hypertrophic, fibrotic, and vascular myocardial remodelling

The consequences of gradual de-PAB using sutures that hydrolyze with pre-defined kinetics were investigated over time (12 weeks) in mice with an initially comparable degree of PA stenosis, assessed by PPG measures across the PA band at 1 week after surgery (*Figure 1A*). Of note, our PPG measurements are not applicable to sham-treated animals as there is no stenotic PA band in place. Two weeks of RV pressure overload significantly impaired RV and left ventricular (LV) function without affecting HR (*Figure 1B–E* and Supplementary material online, *Figure S1*). Banding of the main pulmonary artery led to medial hypertrophy along with adventitial changes (*Figure 1F*) and were accompanied by increased periostin accumulation in interstitial and perivascular RV regions, suggesting ongoing fibrotic remodelling in the stressed RV (*Figure 1G*). Pressure

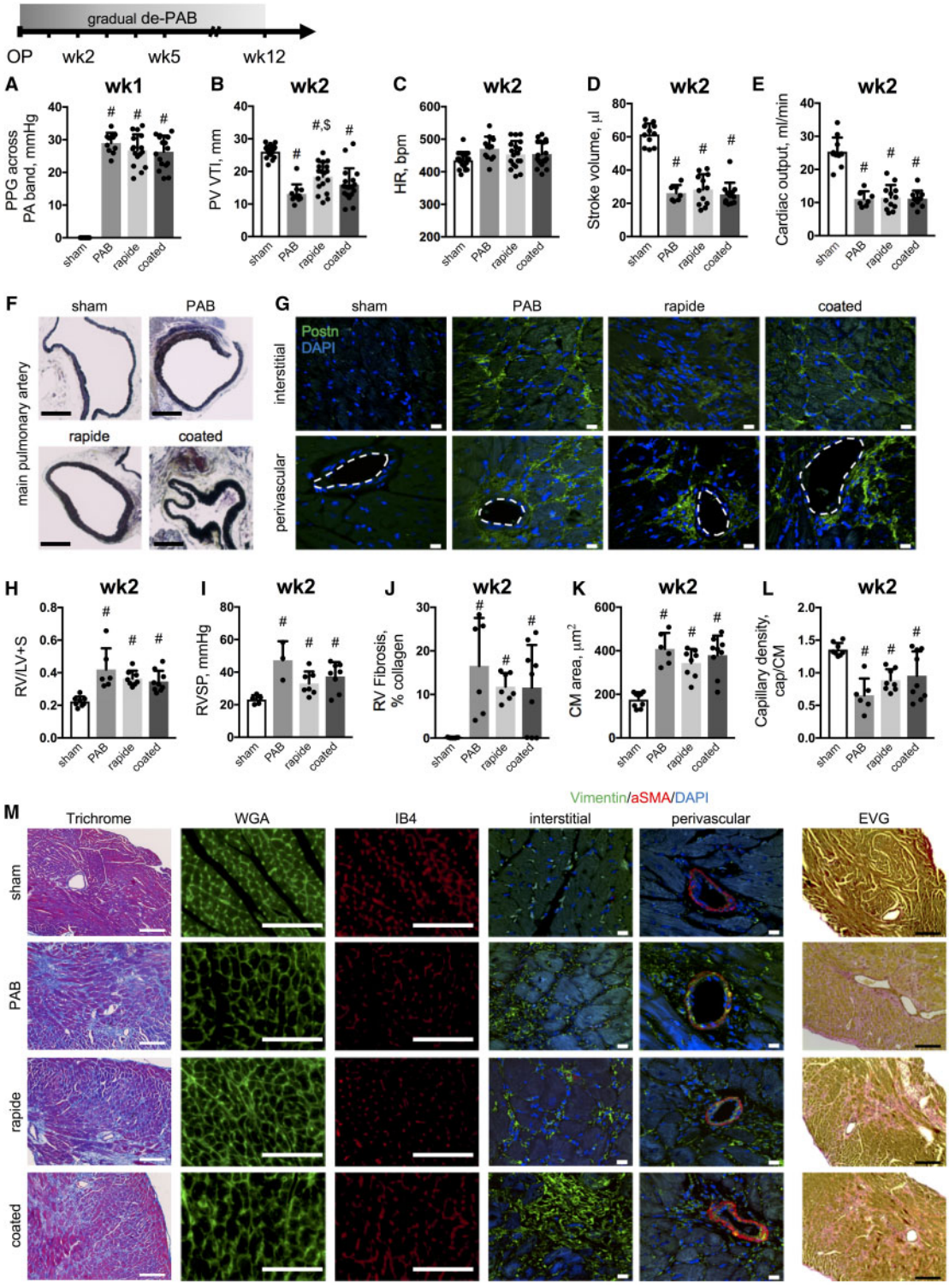

Figure 1 PAB induces RV dysfunction with hypertrophic, fibrotic, and vascular myocardial remodelling. Cardiac function was assessed longitudinally over 12 weeks in mice after sham surgery or PAB with non-absorbable and absorbable sutures. Banding consistency was confirmed by comparable PPG across the pulmonary artery band at 1 week after surgery (*A*). PV VTI (n = 11–18, *B*), HR (n = 11–18, *C*), stroke volume (*D*), and cardiac output (*E*) demonstrate impaired RV function upon PAB with medial thickening of the main pulmonary artery (Russel–Movat–Pentachrome stain, *F*; scale bar =500 µm). Representative images of immunolabelling against periostin (Postn) where dashed lines indicate vessel lumina (scale bar = 10µm, *G*). Fulton's index (RV/(LV + S), *H*). RVSP (n = 3–8, *I*). Quantifications for RV fibrosis (*J*), cardiomyocyte (CM) area (*K*), and capillary density (capillaries to cardiomyocytes, *L*) with representative images for Masson's Trichrome, WGA, IB4, and elastic van Giesson stains (scale bar = 100µm) as well as immunolabelling of Vimentin and aSMA (scale bar = 10µm) (*J*). n = 6–18 animals per group. One-way ANOVA followed by Tukey's multiple comparison *post hoc* test was performed. $^{\#}P < 0.05$ vs. sham; $^{\$}P < 0.05$ vs. PAB.

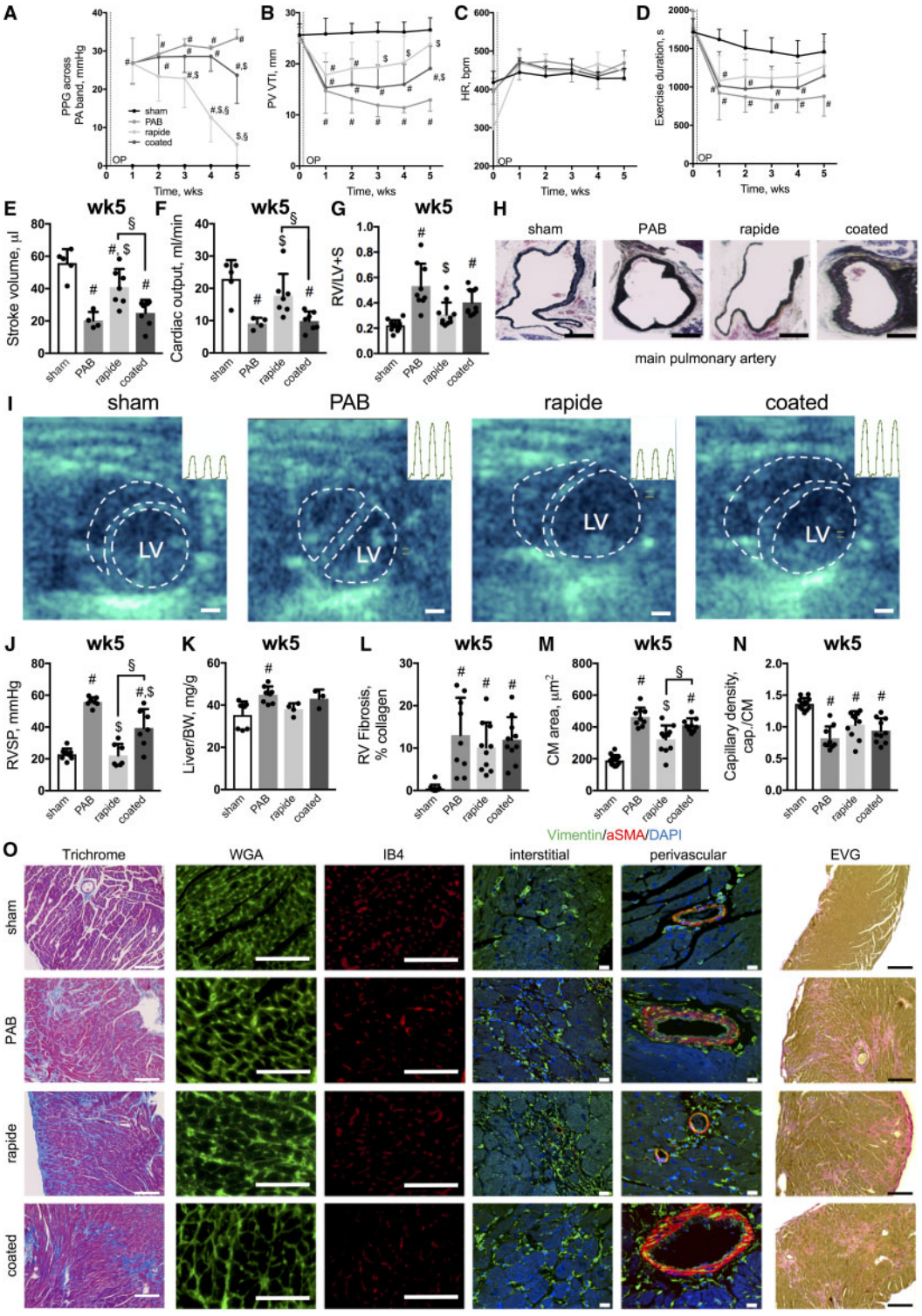

Figure 2 Gradual de-PAB improves RV function and reverses RV hypertrophy. PPG measures across the pulmonary artery band (mmHg, *A*), PV VTI (*B*), heart rate (*C*), exercise duration (*D*), stroke volume (*E*) (n = 4–7), cardiac output (*F*; n = 4–7), and Fulton's index (*G*). Representative images of the main pulmonary artery (Russel–Movat–Pentachrome stain, *H*) (scale bar: 500µm) and echocardiograms at 5 weeks after surgery—dashed lines indicating RV and LV chamber cavity—with intra-cardiac RV pressure traces for three cardiac cycles (inlays, *I*) (scale bar = 1 mm). RVSP (*J*) and Liver-to-bodyweight ratio (*K*) (n = 3–8). Quantifications of RV fibrosis (*L*), cardiomyocyte (CM) area (M) and capillary density (capillaries to cardiomyocytes, *N*) with representative images for Masson's Trichrome, WGA, IB4, and elastic van Giesson stains (scale bar = 100µm) as well as immunolabelling of Vimentin and aSMA (scale bar = 10µm) (*O*). n = 3–15 animals per group and timepoint. (Repeated measure) Two-way or one-way ANOVA followed by Tukey's multiple comparison *post hoc* test was performed. $^{\#}P < 0.05$ vs. sham; $^{\$}P < 0.05$ vs. PAB; $^{\S}P < 0.05$ rapide vs. coated.

overload further caused RV hypertrophy (*Figure 1H*) with increased RV pressure differences among the absorbable band groups (*Figure 1I*). Those changes were accompanied by increased RV collagen accumulation in interstitial and perivascular regions (*Figure 1J* and *M*), cardiomyocyte hypertrophy (*Figure 1K and M*), and decreased capillary density (*Figure 1J* and *M*). Vimentin was used as a broad fibroblast marker to demonstrate that fibroblasts—and not only extracellular matrix molecules such as collagens (Trichrome stain) or elastic fibres (EVG stain)—were present in RV tissue specimen from all groups. Of note, fibroblasts did not co-express aSMA at this timepoint, demonstrating that they are not activated myofibroblasts.[5] Elastic fibres were localized in both, perivascular and interstitial regions in all banding groups (*Figure 1M*).

3.2 Gradual de-PAB improves RV function and reduces RV hypertrophy

Next, we demonstrated that suture hydrolysis led to gradual de-PAB in mice over time with distinct time kinetics for rapide and coated bands (assayed by PPG, *Figure 2A*) along with a concomitant improvement in RV and LV function at around 3 (rapide) or 5 weeks (coated) after surgery, respectively (*Figure 2B–F* and Supplementary material online, Figure *S1*). Similarly, the initial impairment in exercise capacity after sham surgery or PAB improved over time (*Figure 2D*). The functional improvement during gradual de-PAB was accompanied by a reduction in RV hypertrophy as the first 'reverse-remodelling event' (*Figure 2G*) along with reversal of medial thickening in the main pulmonary artery (*Figure 2H*). Furthermore, septal flattening was mitigated in rapide banded mice (*Figure 2I*) along with decreased RV systolic pressures (RVSP; *Figure 2I* and *J*). Of note, 5 weeks of chronic RV pressure overload with non-absorbable sutures led to some degree of mortality ($n = 3$ mice), while no mortality was observed in the de-PAB groups. Due to the observed mortality of some PAB mice at 5 weeks, as well as the severe RV dysfunction, severely reduced exercise capacity, increased RV pressures, septal flattening, RV fibrosis, and liver congestion (*Figure 2K*)—all features of RV failure—observed in the rest of the PAB mice, we were unable to capture data points beyond 5 weeks after the initial surgery in PAB animals with non-absorbable sutures.

On a structural level, increased interstitial and perivascular collagen accumulation (*Figure 2L* and *O*) was observed in all banding groups 5 weeks after surgery, whereas cardiomyocyte hypertrophy decreased in the rapide group only (*Figure 2M* and *O*) without changes in capillary density (*Figure 2N* and *O*), pointing towards cardiomyocytes as the cell type that first responds to afterload reduction. Accordingly, Vimentin$^+$ aSMA$^-$ fibroblasts and elastic fibres were presented in interstitial and perivascular regions of all banding groups (*Figure 2O*). These data suggested that the initial improvement in RV function during gradual afterload reduction primarily depended on cardiomyocyte rather than fibrotic or vascular reverse-remodelling events. In other words, despite the presence of cardiac fibrosis and capillary density reduction, the RV function improved as a result of a reduction in afterload and cardiomyocyte hypertrophy.

3.3 RV dysfunction is fully reversible with reduced CM hypertrophy preceding the reverse-remodelling of fibrotic or vascular events upon gradual de-PAB

We further demonstrate that once the increased afterload burden was completely removed (assayed by PPG, *Figure 3A*), RV and LV dysfunction (*Figure 3B–E* and Supplementary material online, Figure *S1*) including exercise capacity (*Figure 3C*) fully recovered. Similarly, RV hypertrophy (*Figure 3F*) and RVSP (*Figure 3G*) normalized. Interestingly, only animals with a coated PA band showed a residual increase in RV weight ratio, likely because of significant residual extracellular matrix accumulation in both, interstitial and perivascular regions (*Figure 3H* and *K*), while cardiomyocyte size completely reversed (*Figure 3I* and *K*). In contrast, myocardial remodelling in rapide-banded animals was fully restored, as demonstrated by minimal signs of fibrosis (*Figure 3H* and *K*), normalization of CM hypertrophy (*Figure 3I* and *K*), and recovered capillary density (*Figure 3J* and *K*). Fibrosis was still significantly increased and capillary density significantly reduced in the coated group and Vimentin$^+$ aSMA$^-$ fibroblast and elastic fibres were still abundantly present (*Figure 3K*). Altogether, these data demonstrate that RV dysfunction and structural myocardial remodelling are fully reversible with hypertrophic reverse-remodelling preceding fibrotic and vascular density normalization once the increased afterload burden is relieved.

In order to identify key molecular components underlying RV recovery from pressure overload, we performed gene array analyses on RV tissue samples and determined differentially expressed genes ($P < 0.05$, fold change < -2 or >2) for 2 vs. 5 weeks PAB (gene expression programme representing functional worsening, $n = 2$), 2 vs. 5 weeks rapide (gene expression programme representing functional improvement, $n = 2$) and sham vs. 5 weeks rapide PAB group (genes regulated after recovery, $n = 2$–4). Hypothesizing that only genes regulated during functional improvement exclusively can account for beneficial reverse-remodelling processes, we identified 1097 de-regulated transcripts, including genes known to be altered during cardiac remodelling (*Myh6*, *Tgfb1*, *Pdk2*, *Brd4*) (*Figure 3J*). Out of those 1097 candidates, 961 genes were associated with gene ontology (GO) terms. GO analysis revealed significance for growth factor response regulation, protein lipidation, immune response regulation, and apoptosis regulation as processes underlying functional RV improvement (*Figure 3M*). Further, normalization in RV energy metabolism was observed (Supplementary material online, Figure *S2*). The gene expression data for candidates associated with RV recovery is shown (*Figure 3N*) and candidate genes have been validated via qPCR (Supplementary material online, Figure *S3*) with GAPDH as endogenous control. While GAPDH is a gene involved in glucose metabolism, we observed stable expression over time and amongst the different treatment groups, and therefore, deemed it to be an appropriate endogenous control for our experiments. Particularly noticeable is the differential regulation of members of the fibroblast growth factor family (FGFs) involved in tissue repair and regeneration as well as regulation of cardiomyocyte hypertrophy. *Figure 4* summarizes the observed sequence of changes in RV and LV function and histology during RV recovery from pressure overload.

4. Discussion

In this study, we have established a novel pre-clinical mouse model to study RV recovery from pressure overload. The data herein demonstrate that RV dysfunction and structural remodelling are completely reversible once the increased afterload burden is relieved. Restoration of RV function was linked to normalization of RV hypertrophy and RV pressure that preceded fibrotic and vascular reverse-remodelling events. On a sub-cellular level, growth factors, immune modulators, genes involved in energy metabolism as well as apoptosis mediators were identified as major regulators underlying functional RV improvement.

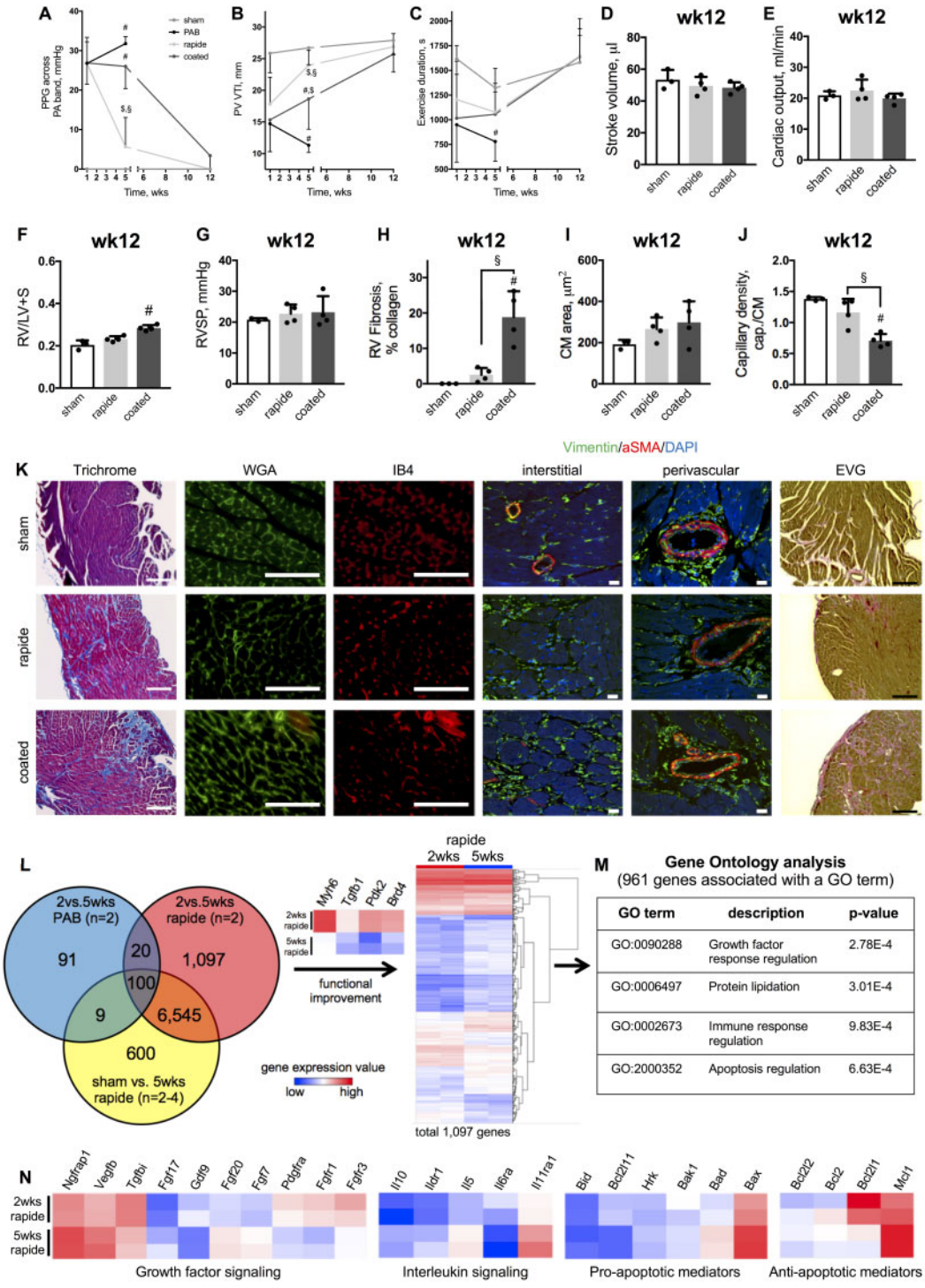

Figure 3 RV dysfunction is fully reversible with hypertrophic preceding fibrotic and vascular reverse-remodelling after gradual de-PAB. PPG across the pulmonary artery band (*A*), PV VTI (*B*), and exercise duration (*C*) over 12 weeks. Stroke volume (*D*), cardiac output (*E*), and Fulton's index (*F*) with RV systolic pressure (*G*). Quantifications of RV fibrosis (*H*), CM area (*I*), and capillary density (capillaries to cardiomyocytes, *J*) with representative images for Masson's Trichrome, WGA, IB4, and elastic van Giesson stains (scale bar = 100µm) as well as immunolabelling of Vimentin and aSMA (scale bar = 10µm) (*K*). Venn diagram showing differentially regulated genes ($P < 0.05$, fold change < -2 or >2) for each possible comparison and a heat map of gene expression values (log2) for differentially regulated genes when comparing PAB with 2 vs. 5 weeks rapide sutures. Genes associated with cardiac remodelling (*Myh6, Tgfb1, Pdk2,* and *Brd4*) are highlighted (*L*). GO analysis of 1097 genes underlying functional improvement, whereof 961 genes were associated with GO terms (*M*). Relative expression of selected differentially regulated genes associated with the indicated cellular processes (*N*). n = 3–4 animals for each group at the 12-week timepoint, n = 2 animals underwent gene array analysis. Repeated measures two-way or one-way ANOVA followed by Tukey's multiple comparison *post hoc* test was performed. $^{\#}P < 0.05$ vs. sham; $^{\S}P < 0.05$ rapide vs. coated. Heatmaps: blue—low expression value; red—high expression value.

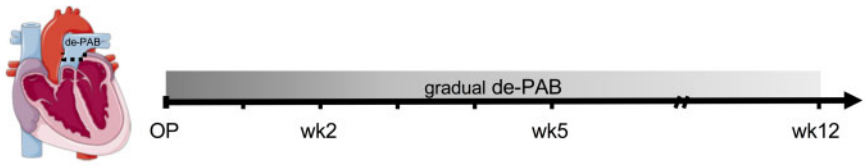

	wk2	wk5	wk12
rapide (vs. sham)	↑ RV pressure ↓ RV function ↓ LV function RV hypertrophy RV fibrosis ↓ RV cap. density	normalized RV pressure normalized RV function normalized LV function normalized RV hypertrophy RV fibrosis ↓ RV cap. density	complete structural and functional normalization
coated (vs. sham)	↑ RV pressure ↓ RV function ↓ LV function RV hypertrophy RV fibrosis ↓ RV cap. density	↑ RV pressure ↓ RV function ↓ LV function RV hypertrophy RV fibrosis ↓ RV cap. density	incomplete structural yet complete functional normalization

↑ increased vs. sham
↓ reduced vs. sham

Figure 4 The major events in RV recovery from PH-associated pressure overload occur in defined sequence. Key changes to RV structure and function during RV recovery summarized for rapide and coated absorbable bands over time (in weeks). ↑, increased vs. sham; ↓, decreased vs. sham; cap., capillary; CM, cardiomyocyte; LV, left ventricular; PPG, peak pressure gradient across pulmonary artery band; RV, right ventricular.

The remarkable capability of the RV to recover after an abrupt normalization in afterload is clinically well documented in patients after surgical removal of pulmonary thrombi[21] or lung transplantation.[6] In those patients though, an impaired LV function has recently attracted some attention resulting in pulmonary oedema development and acute LV failure. In the acute phase after transplantation, extracorporeal membrane oxygenation is, therefore, frequently used to bridge and prime the compromised LV to increased volumes.[22] Our model in contrast, by using absorbable sutures in a surgical PAB mouse model with initially fixed RV afterload, rather leads to a gradual instead of an abrupt decrease in RV afterload that best mimics the process of RV recovery from chronic pressure overload, which would be expected with pharmacological approaches that reverse pulmonary vasculature remodelling.[19] Our model of gradual reduction in RV afterload allows the LV to adjust, therefore offers unparalleled insights into RV recovery without confounding factors of a severely underperforming LV. While the RV dysfunction is thought to be completely reversible in many patients after lung transplantation,[8,9] there seems to be a patient sub-population, however, that does not fully recover functionally after lung transplantation[23] and identifying those individuals preoperatively in order to assign them to heart–lung transplantation is an area of major clinical importance.[5] Our model provides a solid basis for mechanistic studies in this field.

The temporal sequence of RV reverse-remodelling events—once the afterload burden is relieved—and whether RV fibrosis and vascular changes are completely reversible are incompletely understood.[12,13] Cardiomyocytes have been suggested as the cell type that immediately responds to changes in load in a PH sheep model in which the remodelled RV is acutely unloaded mechanically via small implantable ventricular assist devices.[24] In this sheep model, reverse-remodelling of cardiomyocyte hypertrophy rather than a reduction in fibrosis has been observed.[25] Further data from transaortic constriction mouse models with cardiac unloading through removal of the surgical stenosis support the above finding of hypertrophic prior to fibrotic and vascular reverse-remodelling in the heart.[26] Of note, surgical de-banding was found to be technically challenging and was associated with a high mortality (up to 20%[26]) since the connective tissue that surrounded the stenotic band precluded a complete stenosis removal. This was documented by the measurement of a persistent PPG across the former band even 4 weeks after surgical stenosis removal.[26] Our novel de-PAB model is superior to the 'surgical stenosis removal model' as the sutures hydrolyze completely over time, leaving no measurable PPG at the stenosis site. This is crucial to achieve full functional RV recovery.

While the molecular mechanisms underlying improvement in RV function upon afterload alleviation are unknown,[12] it is important to mention here, that the hypertrophic reverse-remodelling with decreasing cardiomyocyte size that we observed is firmly tied to reductions in afterload. As long as there is a persistent and chronic high afterload burden, cardiomyocyte hypertrophy is likely key in maintaining cardiac function and coupling of the ventricular–arterial circuit.[27] Similarly, our studies do not solve the recent debate about whether RV fibrosis impairs RV function in PAH and whether it should be a therapeutic target.[13,28,29] Our finding that the RV function and exercise capacity normalize in the presence of persistent RV fibrosis suggest that cardiomyocytes can perform normally despite an altered matrix but only if the afterload burden is reduced. Therefore, our findings do not make research strategies focusing on ways to improve RV adaptation to a persistently increased RV afterload redundant, but point to the 'self-healing' potential of the RV and emphasize the importance of efforts to develop strategies to reduce and reverse the occlusive pulmonary vasculopathy in PAH.

Identifying genes and pathways that are exclusively regulated in the improving RV and elucidating the exact role for each of these genes and processes, the timepoints when expression might be crucial as well as factors, such as a genetic susceptibility, that might impair up- or

downregulation of these genes, offers the unique opportunity to understand and modulate the recovery process of the RV. *Vegfb*, for example, has been shown to possess pro-angiogenic properties,[30] linking it to capillary density improvement, while *Tgfbi* and *Pdgfra* are both associated with fibrotic remodelling of the heart,[31,32] all genes differentially regulated in the recovering RV after de-PAB. Our data furthermore point towards a prominent role for fibroblast growth factor (FGF)-signalling in the improving RV. FGFs and their receptors have been described in cardiac development as well as in adult tissue where they mediate metabolic functions, tissue repair, and regeneration, in part, by re-activating developmental signalling pathways.[33,34] FGFs have furthermore been shown to orchestrate the hypertrophic response of cardiomyocytes; and FGF-signalling is explored already as a therapeutic target for cardiac remodelling.[35] These examples illustrate that a better understanding of the intrinsic processes which govern functional RV recovery may uncover ways to pharmacologically strengthen the RV and/or accelerate RV recovery from chronic pressure overload by enhancing intrinsic recovery pathways.

Yet, this study comes with several limitations. First, only male mice were used to reduce experimental variability after PA banding, however, sex and related signalling affect the RV response to changes in load. Second, the small sample sizes in some of the groups due to animals that passed away during the study protocol or missed data due to technical difficulties, wherefore not the entire cohort could be statistically tested (PPG measures, RVSP) is a major limitation of this study. Along the same line, a small total number of animals was assessed by microarray gene expression analysis and was limited to specific subgroups of animals to detect gene expression changes associated with RV improvement. Furthermore, the results presented in this study should be considered as a proof-of-principle study. More mechanistic studies are warranted and underway to assess the mechanical changes within the PA upon de-PAB, identify the molecular mechanism that govern fibrosis resolution, recovery of capillary numbers, and elucidate the signalling events that control hypertrophic and vascular reverse-remodelling processes.

In summary, this is the first study to our knowledge that reports a reliable gradual de-PAB model to study RV recovery from RV pressure overload. Our novel mouse model has the distinct advantage over other 'RV recovery models' in that it offers an unparalleled opportunity to employ mouse genetics to study the role of distinct signalling pathways in a spatiotemporal manner that are essential for the intrinsic recovery process or that might impair full recovery, ultimately leading to strategies which might prevent or delay RV failure in PAH.

By utilizing easy-to-use absorbable sutures that hydrolyze with predefined resorption kinetics, this study will likely provide a solid basis for future studies on functional recovery after de-banding in various organs and disease areas such as recovery of LV failure or cardiac re-perfusion after myocardial infarction.

Supplementary material

Supplementary material is available at *Cardiovascular Research* online.

Authors' contributions

M.B. and Y.M.: surgical procedures, experimental design, analysis of results, and manuscript preparation. X.T., K.I., Y.S., S.P.D., K.K., S.R., and M.K.A.: echocardiography, exercise studies, and tissue isolation. M.J.D. and V.O.K.: data analysis. R.J.M.: results discussion and manuscript preparation. E.S.: experimental design, analysis of results, and manuscript preparation.

Conflict of interest: none declared.

Funding

This work was supported by the Max Kade Foundation, Inc. (M.B.), Stanford Cardiovascular Institute (CVI) (E.S. and S.R.), National Heart Lung Blood Institute (NHLBI) at the National Institute of Health (NIH) R01 HL128734 (E.S. and S.D.P.), Wall Center for Pulmonary Vascular Disease Stanford (E.S., R.M., and K.K.), Pulmonary Hypertension Association (PHA) career development grant (E.S.), Department of Defense grant PR161256 (E.S., S.R., and R.M.).

Data availability

The gene array data used to support the findings of this study will be deposited in the Gene Expression Omnibus (GEO) database repository. All other data used to support the findings of this study are included within the article.

References

1. Rabinovitch M. Molecular pathogenesis of pulmonary arterial hypertension. *J Clin Invest* 2012;**122**:4306–4313.
2. van de Veerdonk MC, Kind T, Marcus JT, Mauritz G-J, Heymans MW, Bogaard H-J, Boonstra A, Marques KMJ, Westerhof N, Vonk-Noordegraaf A. Progressive right ventricular dysfunction in patients with pulmonary arterial hypertension responding to therapy. *J Am Coll Cardiol* 2011;**58**:2511–2519.
3. Benza RL, Miller DP, Barst RJ, Badesch DB, Frost AE, McGoon MD. An evaluation of long-term survival from time of diagnosis in pulmonary arterial hypertension from the REVEAL Registry. *Chest* 2012;**142**:448–456.
4. Rich S, Pogoriler J, Husain AN, Toth PT, Gomberg-Maitland M, Archer SL. Long-term effects of epoprostenol on the pulmonary vasculature in idiopathic pulmonary arterial hypertension. *Chest* 2010;**138**:1234–1239.
5. Westerhof BE, Saouti N, van der Laarse WJ, Westerhof N, Vonk Noordegraaf A. Treatment strategies for the right heart in pulmonary hypertension. *Cardiovasc Res* 2017;**113**:1465–1473.
6. Frist WH, Lorenz CH, Walker ES, Loyd JE, Stewart JR, Graham TP Jr, Pearlstein DP, Key SP, Merrill WH. MRI complements standard assessment of right ventricular function after lung transplantation. *Ann Thorac Surg* 1995;**60**:268–271.
7. Berman M, Gopalan D, Sharples L, Screaton N, Maccan C, Sheares K, Pepke-Zaba J, Dunning J, Tsui S, Jenkins DP. Right ventricular reverse remodeling after pulmonary endarterectomy: magnetic resonance imaging and clinical and right heart catheterization assessment. *Pulm Circ* 2014;**4**:36–44.
8. Kramer MR, Valantine HA, Marshall SE, Starnes VA, Theodore J. Recovery of the right ventricle after single-lung transplantation in pulmonary hypertension. *Am J Cardiol* 1994;**73**:494–500.
9. Kasimir MT, Seebacher G, Jaksch P, Winkler G, Schmid K, Marta GM, Simon P, Klepetko W. Reverse cardiac remodelling in patients with primary pulmonary hypertension after isolated lung transplantation. *Eur J Cardiothorac Surg* 2004;**26**:776–781.
10. Hoeper MM, Benza RL, Corris P, de Perrot M, Fadel E, Keogh AM, Kuhn C, Savale L, Klepetko W. Intensive care, right ventricular support and lung transplantation in patients with pulmonary hypertension. *Eur Respir J* 2019;**53**:1801906.
11. Deuse T, Sista R, Weill D, Tyan D, Haddad F, Dhillon G, Robbins RC, Reitz BA. Review of heart-lung transplantation at Stanford. *Ann Thorac Surg* 2010;**90**:329–337.
12. Lahm T, Douglas IS, Archer SL, Bogaard HJ, Chesler NC, Haddad F, Hemnes AR, Kawut SM, Kline JA, Kolb TM, Mathai SC, Mercier O, Michelakis ED, Naeije R, Tuder RM, Ventetuolo CE, Vieillard-Baron A, Voelkel NF, Vonk-Noordegraaf A, Hassoun PM. Assessment of right ventricular function in the research setting: knowledge gaps and pathways forward. An official American Thoracic Society Research Statement. *Am J Respir Crit Care Med* 2018;**198**:e15–e43.
13. Andersen S, Nielsen-Kudsk JE, Vonk Noordegraaf A, de Man FS. Right ventricular fibrosis. *Circulation* 2019;**139**:269–285.
14. Budas GR, Boehm M, Kojonazarov B, Viswanathan G, Tian X, Veeroju S, Novoyatleva T, Grimminger F, Hinojosa-Kirschenbaum F, Ghofrani HA, Weissmann N, Seeger W, Liles JT, Schermuly RT. ASK1 inhibition halts disease progression in preclinical models of pulmonary arterial hypertension. *Am J Respir Crit Care Med* 2018;**197**:373–385.

15. Boehm M, Novoyatleva T, Kojonazarov B, Veit F, Weissmann N, Ghofrani HA, Seeger W, Schermuly RT. Nitric oxide synthase 2 induction promotes right ventricular fibrosis. *Am J Respir Cell Mol Biol* 2019;**60**:346–356.
16. Urashima T, Zhao M, Wagner R, Fajardo G, Farahani S, Quertermous T, Bernstein D. Molecular and physiological characterization of RV remodeling in a murine model of pulmonary stenosis. *Am J Physiol Heart Circ Physiol* 2008;**295**: H1351–H1368.
17. Dunn D, Phillips JJE, Inc, Somerville NJ. Ethicon wound closure manual. 2009. http://www.jnjgateway.com/public/NLDUT/Wound_Closure_Manual1.pdf (1 October 2019, date last accessed).
18. Desai KH, Sato R, Schauble E, Barsh GS, Kobilka BK, Bernstein D. Cardiovascular indexes in the mouse at rest and with exercise: new tools to study models of cardiac disease. *Am J Physiol* 1997;**272**:H1053–H1061.
19. Spiekerkoetter E, Tian X, Cai J, Hopper RK, Sudheendra D, Li CG, El-Bizri N, Sawada H, Haghighat R, Chan R, Haghighat L, de Jesus Perez V, Wang L, Reddy S, Zhao M, Bernstein D, Solow-Cordero DE, Beachy PA, Wandless TJ, Ten Dijke P, Rabinovitch M. FK506 activates BMPR2, rescues endothelial dysfunction, and reverses pulmonary hypertension. *J Clin Invest* 2013;**123**:3600–3613.
20. Reddy S, Zhao M, Hu DQ, Fajardo G, Katznelson E, Punn R, Spin JM, Chan FP, Bernstein D. Physiologic and molecular characterization of a murine model of right ventricular volume overload. *Am J Physiol Heart Circ Physiol* 2013;**304**: H1314–H1327.
21. Fukui S, Ogo T, Morita Y, Tsuji A, Tateishi E, Ozaki K, Sanda Y, Fukuda T, Yasuda S, Ogawa H, Nakanishi N. Right ventricular reverse remodelling after balloon pulmonary angioplasty. *Eur Respir J* 2014;**43**:1394–1402.
22. Verbelen T, Van De Bruaene A, Cools B, Van Raemdonck D, Delcroix M, Rega F, Meyns B. Postoperative left ventricular function in different types of pulmonary hypertension: a comparative study. *Interact Cardiovasc Thorac Surg* 2018;**26**:813–819.
23. Fadel E, Mercier O, Mussot S, Leroy-Ladurie F, Cerrina J, Chapelier A, Simonneau G, Dartevelle P. Long-term outcome of double-lung and heart-lung transplantation for pulmonary hypertension: a comparative retrospective study of 219 patients. *Eur J Cardiothorac Surg* 2010;**38**:277–284.
24. Verbelen T, Verhoeven J, Goda M, Burkhoff D, Delcroix M, Rega F, Meyns B. Mechanical support of the pressure overloaded right ventricle: an acute feasibility study comparing low and high flow support. *Am J Physiol Heart Circ Physiol* 2015;**309**: H615–H624.
25. Verbelen T, Claus P, Burkhoff D, Driesen RB, Kadur Nagaraju C, Verbeken E, Sipido K, Delcroix M, Rega F, Meyns B. Low-flow support of the chronic pressure-overloaded right ventricle induces reversed remodeling. *J Heart Lung Transplant* 2018;**37**:151–160.
26. Merino D, Villar AV, Garcia R, Tramullas M, Ruiz L, Ribas C, Cabezudo S, Nistal JF, Hurle MA. BMP-7 attenuates left ventricular remodelling under pressure overload and facilitates reverse remodelling and functional recovery. *Cardiovasc Res* 2016;**110**:331–345.
27. Vonk Noordegraaf A, Westerhof BE, Westerhof N. The relationship between the right ventricle and its load in pulmonary hypertension. *J Am Coll Cardiol* 2017;**69**: 236–243.
28. Bogaard HJ, Voelkel NF. Is myocardial fibrosis impairing right heart function? *Am J Respir Crit Care Med* 2019;**199**:1458.
29. Crnkovic S, Egemnazarov B, Damico R, Marsh LM, Nagy BM, Douschan P, Atsina K, Kolb TM, Mathai SC, Hooper JE, Ghanim B, Klepetko W, Fruhwald F, Lassner D, Olschewski A, Olschewski H, Hassoun PM, Kwapiszewska G. Disconnect between fibrotic response and right ventricular dysfunction. *Am J Respir Crit Care Med* 2019; **199**:1550–1560.
30. Kivela R, Bry M, Robciuc MR, Rasanen M, Taavitsainen M, Silvola JM, Saraste A, Hulmi JJ, Anisimov A, Mayranpaa MI, Lindeman JH, Eklund L, Hellberg S, Hlushchuk R, Zhuang ZW, Simons M, Djonov V, Knuuti J, Mervaala E, Alitalo K. VEGF-B-induced vascular growth leads to metabolic reprogramming and ischemia resistance in the heart. *EMBO Mol Med* 2014;**6**:307–321.
31. Schwanekamp JA, Lorts A, Sargent MA, York AJ, Grimes KM, Fischesser DM, Gokey JJ, Whitsett JA, Conway SJ, Molkentin JD. TGFBI functions similar to periostin but is uniquely dispensable during cardiac injury. *PLoS One* 2017;**12**:e0181945.
32. Gallini R, Lindblom P, Bondjers C, Betsholtz C, Andrae J. PDGF-A and PDGF-B induces cardiac fibrosis in transgenic mice. *Exp Cell Res* 2016;**349**:282–290.
33. Itoh N, Ohta H. Pathophysiological roles of FGF signaling in the heart. *Front Physiol* 2013;**4**:247.
34. Itoh N, Ohta H, Nakayama Y, Konishi M. Roles of FGF signals in heart development, health, and disease. *Front Cell Dev Biol* 2016;**4**:110.
35. Kardami E, Jiang ZS, Jimenez SK, Hirst CJ, Sheikh F, Zahradka P, Cattini PA. Fibroblast growth factor 2 isoforms and cardiac hypertrophy. *Cardiovasc Res* 2004;**63**:458–466.

Translational perspective

The right ventricle (RV) in pulmonary arterial hypertension possesses a remarkable ability to recover after lung transplantation. Yet, some transplant centres prefer a heart–lung instead of lung transplantation when the RV function is severely impaired because knowledge is lacking whether fibrotic and vascular myocardial remodelling are completely reversible once the increased afterload burden is relieved. We have developed a mouse model to study gradual unloading of the RV and identified key molecular components and the timing of RV reverse-remodelling events with the ultimate goal to understand the RV recovery process and identify ways how to support the RV during recovery.